Recent sedimentation in the Black Sea: New insights from radionuclide distributions and sulfur isotopes

Authors' final draft or 'Post-Print' version. The final version was accepted for publication in Deep Sea Research Part I: Oceanographic Research Papers and published by Elsevier (2012)
Cite as: Yuecel, M, Moore, WS, Butler, IB, Boyce, A & Luther, GW 2012, 'Recent sedimentation in the Black Sea: New insights from radionuclide distributions and sulfur isotopes' Deep Sea Research Part I: Oceanographic Research Papers, vol 66, pp. 103-113. DOI: 10.1016/j.dsr.2012.04.007

Recent sedimentation in the Black Sea: New insights from radionuclide distributions and sulfur isotopes

Mustafa Yücel* [1, 2], Willard S. Moore [3], Ian B. Butler [4,5], Adrian Boyce [6], George W. Luther III [1]

(1) College of Earth, Ocean and Environment; School of Marine Science and Policy, University of Delaware, Lewes, DE 19958, USA

(2) Present address: Benthic Ecogeochemistry Laboratory (LECOB), Université Pierre et Marie Curie – Paris VI, CNRS-UPMC FRE 3350, Observatoire Océanologique, 66650 Banyuls-sur-mer, FRANCE

(3) Department of Earth and Ocean Sciences, University of South Carolina, SC 29208, USA

(4) School of Geosciences, University of Edinburgh, West Mains Road, EH9 3JW, UK

(5) ECOSSE (Edinburgh Collaborative of Subsurface Science and Engineering). A Joint Research Institute of the Edinburgh Research partnership in Engineering and Mathematics

(6) SUERC - Scottish Universities Environmental Research Centre, East Kilbride, Glasgow, UK

* Corresponding author: yucel@obs-banyuls.fr

Tel: +33(0)643160901 Fax: +33(0)468881699

Abstract

The Black Sea is the world's largest anoxic-sulfidic marine basin and has unique sedimentation conditions. Recent studies suggested that mass accumulation rates (MAR) in this environment have increased in the past century when compared to the last 2000 years (Unit 1 period). In this paper we test this hypothesis with new MAR data and further explore the relationship between the depositional pattern and pyrite-sulfur isotopic signature. Based on 15 cores sampled in 2001 and 2003, our dataset comprises radioactive isotopes (^{210}Pb, ^{226}Ra, ^{137}Cs) and sulfur stable isotopes ($\delta^{34}S_{VCDT}$) along with organic, inorganic carbon and pyrite-sulfur. We calculated MARs using ^{210}Pb profiles and/or Chernobyl-derived ^{137}Cs horizon buried in the sediment column. Our turbidite-free deep basin sediment MARs (61 to 76 g m^{-2} y^{-1}) agreed with the previous results (50-100 g m^{-2} y^{-1}) and confirm the view that MARs of the deep Black Sea basin have been increasing. A unique feature of our dataset was the presence of Chernobyl-derived radionuclides below up to 20 cm thick turbidite layers (deposited between 1986-2003), which enabled us to compute MARs for these coring locations. MARs were 1120 ± 103 and 5230 ± 125 g m^{-2} y^{-1} for the last two decades in two turbidite-impacted western central basin cores, 20-100 times the long-term rates of the deep basin. This fast depositional pattern was reflected in the geochemical and isotopic data as well. Turbidites had isotopically heavier pyrite-sulfur compared to the Unit 1-type water column formed pyrite. This is probably because the turbidites originated from slope and transported slope pyrite isotopic signature to the deep basin. Diagenetic effects within the turbidite can make pyrite-sulfur even heavier. These tightly linked results demonstrate the importance of turbidites in recent sedimentation of the Black Sea.

Keywords: Black Sea, sediment, mass accumulation rate, pyrite, sulfur isotope

1. Introduction

The Black Sea is a unique marine environment with permanently anoxic and sulfidic deep waters (Oguz et al., 2005). The sediments depositing under these conditions have been of interest for many decades for their distinctive depositional history (Ross et al., 1970; Mitropolsky et al., 1982). Ross et al. (1970) identified three layers in the uppermost several meters of the anoxic basin sediments: Unit 1, comprising about the uppermost 30 cm of the sediment column, is rich in pyrite, plankton-derived carbonates, and has relatively low levels of organic carbon. Below this layer is Unit 2; about 40 cm thick, with high levels of organic carbon (up to 20%) and low carbonate content. Under these layers lie Unit 3 sediments, which are very low in organic carbon (< 1%).

Sediments from the base of Unit 1 were dated to be 2000-3000 years bp (radiocarbon age) using the accelerator mass spectrometry (AMS) ^{14}C technique (Jones, 1990; Calvert et al., 1991). These ages, however, were a factor of 2-3 times older than the conventional lamina counting method (based on two alternating white and dark layers which were thought to correspond an annual cycle) (Hay, 1988). In order to reconcile the difference, Buesseler and Benitez (1994) and Crusius and Anderson (1992a) used both the ^{210}Pb dating technique and an improved lamina counting method to compare the age of surficial sediments. They concluded that lamina deposition was not necessarily annual. Crusius and Anderson (1992b) also showed that ^{210}Pb was immobile under anoxic conditions of

the Black Sea sediments, proving that the Pb-based technique is more reliable to determine recent mass accumulation rates (MAR), and hence sedimentation processes, across the Black Sea. Following on, a number of studies in the past two decades published ^{210}Pb-based MAR values (Moore and O'Neill, 1991; Gulin, 2000; Gulin et al., 2002, 2003; Teodoru et al., 2007). A major result of these efforts was that the Pb-derived MARs for the last 100 years (50-100 g m^{-2} y^{-1}), were higher than ^{14}C derived rates (30-40 g m^{-2} y^{-1}), which averaged over the past 1000-2000 years. This result was interpreted as an increase in accumulation rates over the past century (Buesseler and Benitez, 1994; Gulin, 2000).

Considerable quantities of reactor-derived radionuclides were introduced to the Black Sea water column and sediments following the 1986 Chernobyl (Ukraine) nuclear reactor meltdown. These nuclides included ^{144}Ce ($t_{1/2}$=0.7 y) ^{134}Cs ($t_{1/2}$=2 y), ^{137}Cs ($t_{1/2}$=30 y); they were found both in sediment traps (Buesseler et al., 1987; Hay and Honjo, 1989) and surface sediments (Moore and O'Neill, 1991; Crusius and Anderson, 1992; Buesseler and Benitez, 1994). ^{137}Cs, with half-life of 30 years, should still be detectable in the cores and hence the signal from this nuclide can be used as a time marker. ^{226}Ra and ^{210}Pb were not released as a result of the accident but their activities were unusually high in the surface layers of cores from the deep basin collected in 1988 (Moore and O'Neill, 1991). Most of these surface layers were defined as "fluff" due their organic-rich nature and porosities higher than 0.96 (Cowie and Hedges, 1991; Moore and O'Neill, 1991) and are thought to represent the remains of high-productivity events in the Black Sea, which could have stripped radionuclides from the surface waters.

Another avenue of Black Sea sediment research has targeted the Sea's use as an analogue for the Precambrian sulfidic ocean (Canfield, 1998). Pyrite and its isotopic composition, expressed as $\delta^{34}S_{VCDT}$, proved to be a useful tracer of processes in past oceanic anoxic-sulfidic conditions and is calculated as

$$\delta^{34}S_{VCDT} = [(^{34}S/^{32}S)_{sample}/(^{34}S/^{32}S)_{VCDT} - 1] * 1000 \qquad \text{(Equation 1)}$$

Where VCDT is the reference material. $\delta^{34}S_{VCDT}$ can be used to determine whether pyrite had formed in the sediment or in the water column before deposition (Lyons, 1997). For example, in the Unit 1 sediments of the anoxic Black Sea basin, $\delta^{34}S_{VCDT}$ of pyrite in surface sediments is constant at about -40 ‰ (Lyons, 1997; Wijsman et al., 2001), which is close to the $\delta^{34}S_{VCDT}$ of dissolved sulfide in the upper part of the anoxic-sulfidic water column (Neretin et al., 2003). In the depths of the sediment column, diagenetic processes become more important. In this case, the pyrite formed within the deeper sediment is isotopically heavier than Unit 1 pyrite. In addition, according to Lyons (1997), $\delta^{34}S_{VCDT}$ values are typically about -25 to -30 ‰ for turbiditic sections of deep Black Sea cores. These turbidites have been relatively understudied in the Black Sea; however, recently, Konovalov et al. (2007) and Yucel et al. (2010a, b) documented the geochemical impact of turbidites in the western deep basin with detailed porewater and solid phase geochemical data. Specifically, these studies showed that turbidites bring reactive iron (III) oxides to sulfidic deep basin and cause the oxidation of porewater hydrogen sulfide to elemental sulfur, which can accumulate to levels close to those of pyrite-sulfur.

In the light of this background, we identify two major gaps in our knowledge regarding Black Sea sediments: (i) the hypothesis of increasing MARs in the Black Sea needs to be better constrained, especially with data from the central and eastern basin (ii) there has not been a combined discussion of radioactive isotopes and sulfur stable isotopes distributions in a given core; such a synthesis would give a more complete picture on the effect of depositional pattern (slow/fast or turbidite) to pyrite accumulation and its isotopic signature. As an effort to address these two issues, here we present a dataset comprising both radioactive isotopes (^{210}Pb, ^{226}Ra, ^{137}Cs) and sulfur stable isotopes ($\delta^{34}S_{VCDT}$) along with geochemical parameters (organic, inorganic carbon and pyrite-sulfur) from recently deposited Black Sea sediments. Based on these data, we present and discuss new MAR values covering the entire Black Sea basin. In addition to the spatial coverage of our cores, a strength of this dataset is the new information on the Chernobyl-derived radionuclides in the sediment column. This enabled us to derive MARs even if the core was affected by turbidites deposited after the Chernobyl accident, which makes the calculation of MAR by the ^{210}Pb method impossible.

2. Methods

2.1 Sediment Sampling

Sediment cores were retrieved with a box core and multicorer during two cruises by R/V Knorr to the Black Sea in May/June 2001 (Leg 2) and April/May 2003 (Legs 8 and 9). The box core was used in 2001 and the multicorer in 2003. Details of coring locations are

presented in Figure 1 and Table 1. Sampling was restricted to western Black Sea in 2001 (5 cores) and the entire basin was sampled in the 2003 cruise (10 cores). The 15 cores represent 12 different locations in the Black Sea shelf (3 stations), slope (1 station) and the deep basin (8 stations). All cores were sectioned in 1-cm intervals on board for radionuclide (^{210}Pb, ^{226}Ra, ^{137}Cs) and porosity analyses. In the 2003 cruise, cores from four deep-basin stations (from a different corer in the same multicore) were also sectioned under O_2-free atmosphere for solid phase sulfur speciation, sulfur isotopes, and organic/inorganic carbon analyses. The majority of these latter analyses and other solid phase data on these cores are discussed by Yücel et al. (2010a, b), except for sulfur isotopes, which are presented for the first time here along with reproduced pyrite-sulfur data. In addition to the visual core logs, the turbidite layers in the cores were identified based on the fact that they were enriched in reactive iron and elemental sulfur, (Yucel et al 2010a), with low ^{210}Pb activity (see section 2.2) and with the pyrite sulfur isotope signature of shelf/slope sediments (see section 2.4).

2.2 Radionuclides and Mass Accumulation Rate (MAR) Calculation

For radionuclide analyses, the wet samples were packed into plastic petri dishes that matched the diameter of the detector and sealed. The ^{210}Pb ($t_{1/2}$ = 22.3 yr), ^{226}Ra ($t_{1/2}$=1600 yr), and ^{137}Cs ($t_{1/2}$ = 30 yr) activities were determined using a low energy, planar germanium detector (Ducat and Kuehl, 1995). Standard soil samples purchased from the National Institute of Standards and Technology were used for the calibration of the detector. Gamma peaks representing ^{226}Ra were monitored to determine the supported activity of ^{210}Pb in the samples. All ^{210}Pb data were corrected for self-absorption effects

employing the procedure of Cutshall et al. (1983). The raw count data were converted to activities using the program HYPERMET (Philips and Marlow, 1976). Measurement uncertainity was 5-10% for radionuclide activities. From the weight loss on drying at 80 ºC, assuming sediments dry density of 2.5 g cm^{-3} (Buesseler and Benitez, 1994) and a porewater salinity of 22; the porosity of the sediment section was determined after correcting for the salt content of the pore water.

Excess (or unsupported) ^{210}Pb activity was calculated by subtracting ^{226}Ra activity from total ^{210}Pb activity, here designated as $^{210}Pb_{ex}$. In the absence of bioturbation, as is the case for the anoxic basin sediments of the Black Sea, the following relation describes the depth-related $^{210}Pb_{ex}$ activity (Appleby and Oldfield, 1992):

$$A(z) = A_0 \exp(-\lambda z/S) \qquad \text{(Equation 2)}$$

where A(z) is the activity of $^{210}Pb_{ex}$ in dpm g^{-1} at depth = z, A_0 is the initial $^{210}Pb_{ex}$, λ is decay constant for ^{210}Pb, 0.0311 y^{-1} and S is the sedimentation velocity in cm y^{-1}. Assuming that the initial sediment contains a constant activity of $^{210}Pb_{ex}$ and that the sedimentation rate is constant, equation (2) can be rewritten in terms of cumulative mass z' and MAR (Buesseler and Benitez, 1994):

$$A(z') = A_0 \exp(-\lambda z'/MAR) \qquad \text{(Equation 3)}$$

For each depth interval, Δz, z' is calculated by multiplying Δz with dry bulk density ρ (1-Ø) , Ø being the porosity at a given depth interval and ρ is the dry sediment solids density (2.5 g cm^{-3}, Buesseler and Benitez, 1994). The sediment masses were corrected for the presence of sea salts using the porosity and the typical bottom water salinity of 22 (Buesseler and Benitez, 1994).

Fitting an exponential curve to equation (3) in a core thus allows the computation of MAR for that depth interval assuming that the model assumptions are valid. For those cores where the model assumptions were violated, i.e. when the cores had subsurface $^{210}Pb_{ex}$ peaks and /or contained a turbidite layer, we used the subsurface Chernobyl-derived nuclide peaks (if present) to calculate MARs since 1986.

2.3 Total Organic/Inorganic Carbon

Solid phase carbon analyses were applied to four deep basin cores from the 2003 sampling: 8-23, 8-07, 8-19 and 8-30. The concentration of total organic carbon (TOC) was determined after removing carbonates (inorganic carbon) by treating the sediment with 1 N HCl (Cowie and Hedges, 1991; Nieuwenhuize et al., 1994). About 3-10 mg of dried subsamples was weighed in silver capsules (5 mm in diameter and 9 mm in height) with CAHN microbalance. For each depth section, two replicates were sampled for total carbon analysis and another two were sampled for the HCl treatment. Addition of HCl causes the conversion of carbonates to CO_2. After the end of the reaction, samples were left at room temperature for 1 h to ensure the complete removal of carbonates and then they were dried at 105 °C along with the blanks. After drying was complete, both total

carbon (TC) and HCl-treated samples were analyzed with a Costech elemental analyzer. Total inorganic carbon (TIC) was determined as the difference between total carbon and total organic carbon (i.e. HCl treated). Average percent standard deviations from mean (of all measurements) were 1.5 % for TC and 2.1 for %TOC. Carbon contents are reported as weight percentages per unit sediment dry weight.

2.4 Pyrite-sulfur and its isotopic composition ($\delta^{34}S_{VCDT}$)

These analyses were also performed for the four deep-basin cores: 8-23, 8-07, 8-19 and 8-30. Pyrite-sulfur was leached from the sediments after the removal of acid-volatile sulfides using cold chromium (II) reduction under a nitrogen atmosphere (Fossing and Jørgensen, 1989; Yucel et al., 2010a). The resulting hydrogen sulfide was trapped in basic traps containing 0.1 NaOH, an aliquot of which was analyzed by cyclic voltammetry at a hanging mercury drop electrode. This measurement was used to back-calculate the amount of pyrite sulfur per g dry weight of sediment. Another subset of samples was leached similarly for $\delta^{34}S_{VCDT}$ analysis. After the completion of the reaction, excess zinc acetate was added to the traps to precipitate and fix sulfide as ZnS. After the completion of the precipitation, the samples were transferred to 50 mL test tubes, sealed well and frozen at -20°C. Before the isotopic analysis, ZnS extracts were centrifuged and the supernatant fluid was removed. The samples were resuspended in deionised water, recentrifuged and the second supernatant was removed. The remaining solid was freeze-dried. During the analysis, the samples were oxidised at 1000°C with copper oxide and CO_2 was removed with a pentane trap. The resulting SO_2 was analyzed for its isotopic

content at the SUERC laboratories (Scotland). $\delta^{34}S_{VCDT}$ of a sample is calculated using Equation 1, where VCDT refers to Vienna Canyon Diablo Triolite.

3. Results

3.1 2001 Cores

The five stations from which cores were collected during the 2001 cruise were all situated in the western Black Sea and their radionuclide data are shown in Figure 2. Core B1C6, sampled from southwestern basin margin, displayed two subsurface $^{210}Pb_{ex}$ maxima, one at 8-9 cm and another at 15-16 cm (Figure 2A). ^{137}Cs penetrated down to 10 cm with no maximum in the profile. ^{226}Ra activity was constant with depth around 1.5 dpm g^{-1}. Cores B1C2 and B1C4 were sampled from the northwestern basin margin and their down-core profiles of radionuclide species were similar to each other (Figure 2B and 2C). In B1C2, $^{210}Pb_{ex}$ activity decreased from 14 to almost 0 dpm g^{-1} in the top 4 cm. ^{226}Ra varied between 1.2 to 2 dpm g^{-1} throughout the core. Core B1C4 had $^{210}Pb_{ex}$ activity of about 10 dpm g^{-1} on its uppermost layer and it decreased below 1 dpm g^{-1} after 5 cm depth. ^{226}Ra also varied between 1-2.5 dpm g^{-1}, peaking at the bottom of the core. Both B1C2 and B1C4 had undetectable ^{137}Cs activity throughout.

Cores B1C1 and B1C5 were taken from the western central basin with B1C1 about 9 km north of B1C5. Core B1C1 had a $^{210}Pb_{ex}$ enrichment of about 40 dpm g^{-1} in the uppermost high-porosity layer (with $\emptyset = 0.94$); $^{210}Pb_{ex}$ activity decreased sharply below the top 1 cm of the core (Figure 2D). ^{226}Ra and ^{137}Cs also displayed a slight surface enrichment at the

top 1 cm, below which ^{137}Cs was undetectable and ^{226}Ra was constant around 1.3 dpm g^{-1}. Unlike this core, B1C5 had subsurface maxima for $^{210}Pb_{ex}$, ^{137}Cs and ^{226}Ra activities (100, 8.4 and 5.5 dpm g^{-1}, respectively) at a depth of 6 cm with activities higher than the values of the surface layer. This core apparently overpenetrated causing some of the surface layer to be lost. The porosity of this subsurface maxima layer was also similar to the remaining surface layer at about 0.93. We do not describe them as "fluff" yet since it was defined for layers with porosities equal or larger than 0.96 by Moore and O'Neill (1991). The subsurface maxima of ^{137}Cs, $^{210}Pb_{ex}$, ^{226}Ra, and porosity were apparently the remains of the surface layer enriched in Chernobyl–derived ^{137}Cs and other radionuclides observed in 1988 cores (Moore and O'Neill, 1991). As of 2001, it appears that this layer has been covered by sediments that are still somewhat enriched in ^{226}Ra. Core B1C1, on the other hand, did not show any subsurface enrichments in ^{137}Cs or $^{210}Pb_{ex}$. This core possibly contained a turbidite underneath the surface layer as evidenced from the low and constant activities of $^{210}Pb_{ex}$, and ^{226}Ra.

3.2 2003 Cores

2003 sampling involved 3 stations on the different parts of the Black Sea shelf and data form these cores are shown in Figure 3. Core 9-2 was just offshore the Black Sea side of the Bosporus. $^{210}Pb_{ex}$ activity was about 11 dpm g^{-1} at the surface layer and decreased to less than 1 dpm g^{-1} after 10 cm with a subsurface $^{210}Pb_{ex}$ peak, which coincided with the ^{137}Cs peak at 4 cm (Figure 3A). ^{137}Cs activity displayed a downcore decrease as well from about 3 dpm g^{-1} to non-detectable in the top 10 cm. Core 8-29 (Figure 3B) was on the southern shelf, offshore Sinop (Turkey), and subsurface $^{210}Pb_{ex}$ and ^{137}Cs peaks were

detected at 1.5 cm depth. Here $^{210}Pb_{ex}$ activity reached 44 dpm g^{-1} and ^{137}Cs activity was 12 dpm g^{-1} whereas ^{226}Ra was enriched at the top two cm at about 4 and then decreased to around 1 dpm g^{-1}. On the northern Crimean shelf of the Black Sea, core 8-3 also displayed similar subsurface maxima of $^{210}Pb_{ex}$ activity at 2.5 cm (26 dpm g^{-1}) and ^{137}Cs activity at 3.5 cm (4.6 dpm g^{-1}) (Figure 3C).

Core 9-8 was on the southwestern slope and close to the 2001 core B1C6. As shown in Figure 3D, the top 2 cm of the core had around 32 dpm g^{-1} of $^{210}Pb_{ex}$ and 5 dpm g^{-1} of ^{137}Cs activity. Below 2 cm, both nuclides displayed low activities and ^{226}Ra was constant around 2 dpm g^{-1} throughout the core.

Also shown in Figure 4 are data from two cores of the deep basin: core 8-28 (Figure 3E) and core 8-5 (Fig. 3F). Core 8-28 was close to the southern margin of the deep basin; here $^{210}Pb_{ex}$ activity decreased from 105 dpm g^{-1} at the surface to 0 at 10 cm depth. The uppermost layer had a porosity >0.96, hence this core can be said to have contained "fluff". ^{137}Cs had a subsurface peak at 3.5 cm with an activity of 11 dpm g^{-1}. Interestingly, at 12 cm all radionuclides display subsurface peaks. Core 8-5 was to the north of 8-28, at the center of the anoxic basin, hence the radionuclide activities here were higher as expected from the decreasing effect of clastic dilution. $^{210}Pb_{ex}$ activity was about 400-500 dpm g^{-1} at the surface layer of the core, and peaked in the 3-4 cm interval with 921 dpm g^{-1}. The uppermost 5 cm of core had also high porosities of 0.99-0.97. ^{137}Cs and ^{226}Ra activities also peaked at the 3-4 cm interval with activities 26 and 36 dpm g^{-1}, respectively.

In addition to the radionuclide analyses, we performed solid phase sulfur speciation, $\delta^{34}S_{VCDT}$ and TOC/TIC analysis on the remainder of the 2003 deep basin cores, and, those results are presented separately in Figure 4. Core 8-19, sampled from the southeastern basin margin, had a high porosity fluff layer (0.97) on the top two centimeters of the core. This surface layer also had high $^{210}Pb_{ex}$ activities starting with 168 dpm g^{-1}, below 2 cm depth $^{210}Pb_{ex}$ activity decreases sharply (Figure 4A). All radionuclides had a subsurface maxima around 12 cm, collectively pointing to the presence of the 1986-1988 surface layer at this depth. ^{137}Cs had an activity around 6 dpm g^{-1} here, about 4 times higher compared to the background level of the core. In addition to the 12 cm depth, ^{226}Ra is also enriched in the top cm layer with an activity of 4 dpm g^{-1}. Organic and inorganic carbon levels also showed a surface enrichment at about 5 and 3 %, respectively, and they peaked around 10 cm. This layer possibly corresponds to the 12 cm layer of the radionuclide core and the two cores possibly had gone through different amounts of compaction to yield a slight offset between the depths. Pyrite-sulfur also peaked at this depth, with its $\delta^{34}S_{VCDT}$ becoming more negative downcore from -22 ‰ at 2 cm to -28 ‰ at 10 cm.

Data from core 8-23, sampled from the western basin, are shown in Figure 4B. $^{210}Pb_{ex}$ activity steadily decreased from 210 dpm g^{-1} at the surface to 1 dpm g^{-1} at 10 cm. The subsurface ^{137}Cs and ^{226}Ra peaks were located around 4 cm. ^{137}Cs activity at his depth, 30 dpm g^{-1}, is the highest measured ^{137}Cs activity among the sampled cores of this study. Organic and inorganic carbon decreased downcore and below 11 cm depth a sharp

decrease in carbon levels to a steady value is remarkable. Pyrite-sulfur concentration increased downcore with $\delta^{34}S_{VCDT}$ of pyrite remaining constant between -34 and -38 ‰. Core 8-7, another western central basin core, had a steadily decreasing activity of $^{210}Pb_{ex}$ from a value of 373 dpm g^{-1} at the surface to 0.4 at 10 cm depth (Figure 4C). The 3-4 cm interval contained the subsurface peaks of ^{137}Cs and ^{226}Ra. TOC was enriched at the surface at 9 % and it was about 5 % at the bottom of the core, TIC fluctuated between 4-7 %. Pyrite sulfur concentration was high and variable as well, and its $\delta^{34}S_{VCDT}$ had a minimum of -25 ‰ at 6 cm depth but otherwise it was more negative than -30 ‰.

Core 8-30 (Figure 4D) of the western central basin was within 18 km of stations B1C1 and B1C5 of the 2001 cruise. Here $^{210}Pb_{ex}$ activity decreased abruptly in the top two cm from 186 dpm g^{-1} to about 5 dpm g^{-1}, and stayed at this activity until the 21-22 cm interval, where subsurface maxima of $^{210}Pb_{ex}$, ^{137}Cs and ^{226}Ra were present. Similar to other layers containing deep-basin subsurface radionuclides maxima, this layer probably records deposition between 1986-88 as evidenced by the enriched Chernobyl-derived ^{137}Cs. The uniqueness of this core is the presence of an almost 20-cm thick turbidite. The upper and lower boundaries of this turbidite layer were also enriched in TOC and TIC. Pyrite-sulfur and $\delta^{34}S_{VCDT}$ values also show similar spikes at about 20 cm interval. It is possible that the core used for sulfur speciation work underwent more compaction, resulting in the depth discrepancy. In the turbidite, both pyrite sulfur concentrations were lower and $\delta^{34}S_{VCDT}$ values were more positive compared to the deeper layers of the core. TOC/TIC and the radionuclide data suggest there is normal sedimentation in the uppermost 0-2 cm layer, covering a recently deposited turbidite.

4. Discussion

We analyzed 15 surface sediment cores across the Black Sea basin for $^{210}Pb_{ex}$, ^{137}Cs and ^{226}Ra in order to delineate the recent depositional conditions in this oceanographically unique environment. Four of these cores were also analyzed for carbon contents, sulfur speciation and $\delta^{34}S_{VCDT}$ of pyrite to give a complete picture of the relationship between the depositional pattern and sediment geochemistry.

4.1 Radionuclide distributions, inventories and mass accumulation rates (MAR) across the Black Sea Basin

Calculated MAR values and radionuclide inventories are presented in Table 2. We were able to apply Equation 3 to the data from 6 cores of the deep basin, and their best fit exponential curves are shown in Figure 5. Subsurface ^{137}Cs peaks were used to compute a total of 9 MAR values, allowing us to compare the two different approaches for the three cores.

4.1.1. Shelf

Our shelf cores were all sampled during the 2003 cruise from three different locations: offshore Bosporus (9-2), Crimean Peninsula (8-3) and southern shelf in the vicinity of Sinop (8-29). The uppermost layer of 8-3 and 8-29 did not contain the highest amount of $^{210}Pb_{ex}$ activity; instead a subsurface layer, located beneath the surface layer, had the maximum values. This layer was also enriched in ^{137}Cs (but not in ^{226}Ra). These subsurface peaks are probably due to the unusually high deposition of $^{210}Pb_{ex}$ with ^{137}Cs

after the Chernobyl accident between 1986-88 (Moore and O'Neill, 1991). Mixing of the top 1-2 cm could have caused the constant values of ^{226}Ra activity on the top 2 cm of core 8-29. These $^{210}Pb_{ex}$ distributions clearly violate the assumptions of equation 1; thus, we could not calculate MARs using this model. Instead we assume that the subsurface peak of ^{137}Cs represents the Chernobyl fallout peak (1986); sediment above this layer must have been deposited between 1986 and 2003 (17 years). Dividing the mass of sediment above the Chernobyl layer by 17 years yielded MARs of 978 ± 140, 390 ± 130 and 1673 ± 240 g m^{-2} yr^{-1} for 8-3, 8-29 and 9-2, respectively**,** for the past 17 years. MARs of 8-3 and 9-2 were higher than that of 8-29, which was at a deeper location and further away from the land. $^{210}Pb_{ex}$ and ^{137}Cs inventories are also the lowest in 8-29. Previously reported $^{210}Pb_{ex}$ -based MARs from Black Sea shelf cores range from 425 (Teodoru et al., 2007) to 4000 g m^{-2} yr^{-2} (Gulin et al., 2002, 2003). The highest values were from cores taken in front of river deltas, and our MARs fall within the expected values for Black Sea shelf.

4.1.2 Slope

Core 9-8, the only slope core of this study, displayed constant $^{210}Pb_{ex}$ and ^{137}Cs activity on the top two centimeters, which could indicate mixing, or could be the Chernobyl layer that has not been covered by more recent sediment. The overlying waters and porewaters of 9-8 were sulfidic (Konovalov et al., 2007), which excludes the possibility of bioturbation. At this shelf break setting, subsurface currents could have caused sediment resuspension and thus affected the depth distribution of radionuclides. Due to the small

$^{210}Pb_{ex}$ gradient and the lack of the subsurface radionuclide peaks, we could not calculate MARs for this core.

4.1.3. Basin Margin

The southwestern margin core B1C6, located slightly north of 9-8, had a complicated $^{210}Pb_{ex}$ activity profile with two subsurface peaks. ^{137}Cs here penetrated to about 8 cm at a constant activity, suggesting a mixed layer, but the $^{210}Pb_{ex}$ shows distinct structure arguing against mixing. Two marginal cores of the western deep basin, B1C2 and B1C4, had reasonable $^{210}Pb_{ex}$ profiles, which yielded higher MARs (94 ± 44 and 106 ± 10 g m^{-2} yr^{-1}, respectively) compared to the central basin cores (discussed in 4.1.4). Marginal basin core 8-28 had a complicated $^{210}Pb_{ex}$ profile with 3 distinct subsurface maxima, violating the assumptions of equation 1. Here we use the presence of the Chernobyl layer at 4 cm depth to calculate a MAR of 257 ± 37 g m^{-2} yr^{-1}. In spite of the complicated profile, a best fit to the $^{210}Pb_{ex}$ vs cumulative mass plot of 8-28 (figure 5d) gave a good correlation ($R^2 = 0.96$) yielding a MAR value of 178 ± 27 g m^{-2} yr^{-1}, reinforcing the high ^{137}Cs-derived MAR. An explanation for the high MAR of 8-28 could be that the focusing of vertical material transport is enhanced at this portion of the Black Sea as the eastern and western surface gyres meet at the center of the basin (Oğuz et al., 2005), concentrating material here. Nevertheless, the possibility of the presence of turbidites here cannot be excluded due to the shape of the $^{210}Pb_{ex}$ profile.

Core 8-19, in the southeastern corner, had a thick turbidite from 3-13 cm depth; the Chernobyl peak is apparently below this turbidite. Using this peak, a MAR of 2768 ± 111

g m^{-2} yr^{-1} is calculated. Although this is extremely high, it does represent the accumulation rate of sediment in this location for the 17 year period. Using the $^{210}Pb_{ex}$ distribution in the top 4 cm of the core a MAR of 58 g m^{-2} yr^{-1} (best fit not shown) can be calculated but this value does not represent true sedimentary conditions at this setting.

The high MARs in the northwestern margin of the Black Sea anoxic basin may be the result of Danube River and its particle inputs. In the absence of major rivers, such as the southeastern margin of the basin, which is close to a steep continental slope, turbidites are often the agents of elevated sediment accumulation rates. As also discussed in Lyons and Kashgarian (2005), this fast sediment accumulation regime in the Black Sea anoxic basin margin creates a unique geochemical signature in the geological record, which is further complicated by turbidites.

4.1.4. Abyssal Plain

In the central basin, to the northwest of 8-28, core 8-5 has a clear subsurface Chernobyl peak at 4 cm depth. Using the same approach as for other cores with this feature, this yields a MAR of 93 ± 14 g m^{-2} yr^{-1} for the upper 4 cm. This value falls within the higher end of the range of 31-100 g m^{-2} y^{-1} previously reported for deep Black Sea basin sediments > 1000 m water depth. The high $^{210}Pb_{ex}$ inventory of 172 dpm cm^{-2} in this core is the highest measured in this study. From mass balance considerations, Moore and O'Neill (1991) predicted a ^{210}Pb inventory of 70-80 dpm cm^{-2} for the anoxic Black Sea sediments. Most of our deep basin results are close to this range (Table 2), but only the inventory of 8-5 is more than 2 times higher than this value. When considered with the

high MAR of this core, apparently there is increased sedimentation and removal of ^{210}Pb with particles in the central part of the sea, possibly due to the convergence of the two gyres (Oğuz et al., 2005).

Mass accumulations rates (^{137}Cs-based) in the turbidite-free Unit-1 type eastern central sediments were 44 ± 9 g m^{-2} y^{-1} for 8-7 and 117 ± 17 g m^{-2} y^{-1} for 8-23, with similar radionuclide inventories (Table 2). $^{210}Pb_{ex}$-based MARs were close to these values (61 ± 6 and 76 ± 7 g m^{-2} y^{-1} for 8-7 and 8-23, respectively) . We did not find turbidites in the central and eastern central basin, but they were found in western central station cores. We sampled the western central station twice in 2001 (B1C1 and B1C5) and once in 2003 (8-30). B1C1 was 3.5 km to the north of B1C5 and its radionuclide inventories were much lower than B1C5. Only the top layer of B1C1 was enriched in $^{210}Pb_{ex}$ and ^{137}Cs, whereas the rest of the core had constantly low activities. Together with the absence of the subsurface ^{137}Cs and ^{226}Ra peaks showing the 1986-88 deposition horizon, the presence of a turbidite layer here is evident. The MAR calculated using only the surface 4 cm layer was 72 ± 35 g m^{-2} y^{-1}, however we note that this does not represent long-term (more than a decade) sedimentation in this area. B1C5 had a quite different radionuclide distribution with the presence of the subsurface peaks, and the turbidity current that affected cores from just 3.5 km to the north apparently seems like not to have had the same effect here. However, based on the location of the subsurface nuclide peaks (and considering that some of the surface may have been lost due to overpenetration), we calculate a MAR of >1100 g m^{-2} y^{-1}, clearly showing increased sedimentation over the period 1986-2001. The 2003 core 8-30 was 14 km east of B1C5, and this core also had a turbidite layer of almost

20 cm thickness. The location of the Chernobyl peaks was below the turbidite and this gave a MAR of 5200 g m^{-2} y^{-1}. It is difficult to date the turbidite precisely due to the presence of a 1 cm thick fluff layer with high $^{210}Pb_{ex}$ activity covering the turbidites. Nevertheless, the location of high ^{137}Cs and ^{226}Ra layer below the 8-30 turbidite is consistent with a turbidite emplaced after 1988, possibly after the two magnitude >7 earthquakes in northwestern Turkey in 1999 . Turbidite emplacement is apparently quite heterogeneous and thicknesses of the deposited turbidite layers can vary greatly as two cores 14 km apart can have different geochemistries. Nevertheless, the impact of the turbidites in the western central basin is apparent from our data and the extremely high MAR values of the two cores from this location.

In recent decades a number of studies (Buesseler and Benitez, 1994; Gulin, 2000) proposed an increase of the MARs in the Black Sea over time, based on the finding that ^{210}Pb-based MARs of the past 100 years exceed ^{14}C based MARs, which average out a much larger time scale (1000-2000 years). Overall, our calculated ^{210}Pb-based MARs in the turbidite-free cores of the eastern central abyssal plain are 61 and 76 g m^{-2} yr^{-1} (Table 2). Previous work mostly reported MAR values from the western central basin, within the range of 50-100 g m^{-2} yr^{-1} (i.e. Crusius and Anderson, 1992; Buesseler and Benitez, 1994; Gulin, 2000; Teodoru et al., 2007). Our MAR values from the eastern basin suggest that the increase in MARs in the Black Sea is not confined to the western basin. Thus, the previously proposed increase in the mass accumulation in the last 100 years in the Black Sea is shown to be a basin-wide phenomenon. The most likely reason behind the increasing MARs is the eutrophication-induced increasing particle fluxes in the past

several decades. Several lines of evidence from water column Ba and Ra profiles (Falkner et al, 1991; Moore and Falkner, 1999) were used to argue that the removal of these nuclides increased due to increased productivity in the surface waters in the past decades. Teodoru et al (2007) also confirmed this trend through their reconstruction of sedimentary nitrogen and phosphorus fluxes.

Our ^{210}Pb-based sedimentation velocities for the abyssal plain, ranging from 0.25 to 0.48 mm yr^{-1} are also higher than 0.2 mm yr^{-1}, a value considered by Lyons and Kashgarian (2005) and elsewhere as a typical rate for Unit 1 sediments. This is apparently a minimum for this environment, especially after the eutrophication-induced elevated particle fluxes in the region in the past decades. ^{137}Cs-based sedimentation velocities (also shown in Table 2) are even higher, which could be due to a combination of the diagenetic mobility of ^{137}Cs after deposition and our 1-cm sectioning of the core, which might have magnified the error. The error is smaller in the MARs calculated by two methods as the mass of the sediment is taken into account. As far as the sedimentation velocities are concerned, we used our ^{210}Pb-based results as a more reliable indicator of sedimentation velocities since the diagenetic immobility of ^{210}Pb in the anoxic Black Sea sediments was demonstrated by Crusius and Anderson (1992).

4.2 Pyrite $\delta^{34}S_{VCDT}$ in the deep basin

The deposition patterns presented above have a clear imprint on the isotopic signature of the pyrite found in deep basin sediments. Isotopic compositions of pyrite sulfur in the four anoxic basin cores are summarized in Table 3. The $\delta^{34}S_{VCDT}$ of the "normal" deep

Black Sea basin cores (stations 23 and 07) had more negative values (i.e. were isotopically lighter) than the turbidite containing cores from stations 19 and 30. The mean $\delta^{34}S_{VCDT}$ for stations 23 and 07 were -35.7 and -36.3 ‰, respectively (Table 3), close to the value reported by Lyons (1997) (-37.2 ‰) for the pyrite in Unit 1 sediments. Both cores had even lighter pyrite at their surfaces, close to or more negative than -40 ‰, indicating the imprint of the water-column formation of pyrite (Neretin et al., 2000; Wijsman et al., 2001).

The mean $\delta^{34}S_{VCDT}$ in the top 1-19 cm of the station 8-30 core (turbidite) was -24.0 ‰, close to the turbiditic station 19 core's mean value of -24.6 ‰. These values are close to the lower end of the previously reported range for the deep basin turbidites (-25 to -30 ‰) and more positive by 3.0 ‰ compared to the S isotope compositions Lyons (1997) reported for the pyrite forming on the upper slope of the Black Sea basin (-27.6 ‰). Still, as Lyons (1997) also argued, these data point to an upper slope source for the deep basin turbidites. Our radionuclide results also support this conclusion as it seems that turbidites were initially deposited in a region where there was a low initial activity of excess ^{210}Pb, but a more moderate activity of ^{137}Cs. Sediments deposited on the shelf/basin margin during the early 1960's would fit this well. After pyrite bearing the isotopic signature of the slope sediments was deposited in the deep basin, the reactive Fe(III) brought by the turbidite (Yucel et al., 2010b) and subsequent pyrite formation by its reaction with sulfide could utilize more of the sulfide reservoir already depleted in light sulfide, making the resulting pyrite S isotope composition heavier than the slope values, as seen in our data.

In the core 8-30 (Figure 4D), the transition from turbidite layer to Unit 1 sediments at 20 cm depth can be followed from the sulfur-isotope profile as well. The $\delta^{34}S_{VCDT}$ of the pyrite in the old fluff layer at 20-21 cm section is -40.2 ‰, bearing the signature of water column formed pyrite similar to the surfaces of stations 07 and 23. After 21 cm depth, $\delta^{34}S_{VCDT}$ progressively becomes less negative and the mean $\delta^{34}S_{VCDT}$ in the 20-51 cm section was -31.0 ‰. This value is ^{34}S depleted (lighter) compared to the composition of the turbidite layer by 7.0 ‰, demonstrating the contrasting chemistries of the two layers. The change in $\delta^{34}S_{VCDT}$ with depth could be due to the closed system effects that restrict the diffusion of light sulfate from the water column to 20-50 cm depths in the sediment (Jørgensen, 1979). This results in the generation of heavier dissolved sulfide by prokaryotes and its contribution to diagenetic pyrite formation. The diagenetic heavy pyrite formation in this deep layer could also be enhanced by the reduction of Fe(III) in the upper turbidite layer and its subsequent diffusion to the deeper layers to form pyrite.

4.3 Fluff layers in the deep basin

The surface fluff layers, defined as layers with a porosity larger than 0.96, were thickest in the central and eastern central basin sediments (4-5 cm, see Table 2). In the central western basin sediments, only core 8-30 was covered by a 1 cm fluff and others (B1C1 and B1C5) did not have the fluff; however, these cores were collected by box cores, which could have disturbed the fluff layer; we are certain that some of the surface sediments were lost from B1C5. The post-1988 turbidite deposition event(s) in the western basin could also have affected the stability and thickness of the fluff in the western basin.

As indicated by Moore and O'Neill (1991), the surface fluff layers in the cores sampled in 1988 contained high activities of Chernobyl-derived and natural radionuclides, ^{137}Cs, ^{134}Cs, ^{144}Ce, $^{210}Pb_{ex}$, and ^{226}Ra. These surface layers were proposed to have contained the remains of a high-productivity event that occurred between 1986 and 1988, which stripped the radionuclides from surface waters. During 2001 and 2003 we found new surface fluff layers and recognized "old" ones from 1988 first observed by Moore and O'Neill (1991). These old fluff layers were preserved intact with their typical radionuclide enrichments in the deeper layers, covered by turbidites in 8-30 and 8-19, or by normal sedimentation in the rest of the deep basin cores. The 1988 fluff layers and the new ones have similar inorganic and organic carbon content, which are 4-5 fold higher than the rest of the core, as best evidenced in the profiles of 8-30 (Figure 4D). The buried fluff layer of this core also had the signature of water-column forming pyrite. Here, the burial of fluff layers by the turbidites clearly resulted in an enhanced carbon burial in the deep basin. Depending on the sedimentary area affected by the turbidites, this mechanism could be an important factor in the Black Sea carbon cycle. The fluff also plays an important role in the sulfur cycle of the anoxic basin through sulfur incorporation into organic matter (Yucel et al., 2010a). As shown by that study, solid phase organic sulfur concentration can approach that of pyrite in the fluff.

Overall, we suggest that the fluff is an essential property of deep basin Black Sea sediments and its deposition could be as frequent one-two fluff layer formation events per

10-15 years taking into account the time interval between the 1988 sampling of Moore and O'Neill (1991) and this study (2001 and 2003).

5. Conclusions

In this paper we presented new mass accumulation rates (MAR) from cores covering the entire Black Sea basin. We calculated MARs based on ^{210}Pb profiles and the Chernobyl-derived ^{137}Cs horizon buried in deeper layers of the sediment column. Our turbidite-free deep basin sediment MARs (61 to 76 g m^{-2} y^{-1}) agreed with the previous results (50-100 g m^{-2} y^{-1}) and confirm the previously suggested proposal that MARs in the past decades/century have increased when compared to the whole of Unit 1 period (2000 years), likely due to the eutrophication-induced increases in particle inputs to sediments. A unique feature of our dataset was the presence of Chernobyl-derived nuclides below thick (up to 20 cm) turbidite layers (deposited between 1986-2003). These buried features enabled us to compute MAR values for these coring locations, which ranged between 1100 - 5200 g m^{-2} y^{-1} for the last two decades, 20-100 times the background rates of the deep basin, in these turbidite-impacted cores. In the Black Sea, such high MAR values are typically only attained in front of river deltas such as Danube and Coruh [(3000-4000 g m^{-2} y^{-1}, (Gulin et al., 2002, 2003)] showing the intensity of particle transport by turbidity currents, which links the shelf and slope environments to the deep Black Sea.

The radionuclide-based depositional patterns were tightly linked to the geochemical and sulfur isotopic results. Turbidites had isotopically heavier pyrite-sulfur compared to the

Unit 1-type water column formed pyrite. This is probably because the turbidites originated from the slope, thus bringing sediments with a slope isotope signature to the deep basin. Our iron-sulfur data also suggest that the diagenetic effects within the turbidite can make pyrite-sulfur even heavier, as seen in our isotope data. In conclusion, turbidites in the Black Sea deserve further study to better constrain particle fluxes and carbon and sulfur cycling in this environment.

Acknowledgements: This research was supported by grants from NSF (OCE-0096365) and CRDF (UKG2-2645-SE-05). Access to the Isotope Community Support Facility at SUERC was achieved via NERC support (IP/1050/0508 to IBB). We thank to the captain and crew of R/V Knorr, 2001 and 2003 Black Sea cruises and Sena Akcer who collected cores 9-2 and 9-8. This work represents a part of MY's PhD dissertation at the University of Delaware. MY acknowledges UPMC-TOTAL Foundation's funding for his postdoctoral stay at LECOB, during which part of this manuscript was drafted.

References

Appleby, P.G, Oldfield F., 1992. Application of lead-210 to sedimentation studies, in: Ivanovich, M., Harmon, R.S. (Eds.), Uranium Series Disequilibrium (2nd edition), Oxford.

Buesseler, K.O., Livingstone, H.D., Honjo, S., Hay, B.J., Manganini, S.J., Degens, E., Ittekkot, V., Izdar, E., Konuk, T., 1987. Chernobyl radionuclides in a Black Sea sediment trap. Nature 329, 825-828.

Buesseler, K.O., Benitez, C.R., 1994. Determination of mass accumulation rates and sediment radionuclide inventories in the deep Black Sea. Deep Sea Res. Pt. I 41, 1605-1615.

Canfield, D. E., 1998. A new model for Proterozoic ocean chemistry. Nature 396, 450-453.

Calvert, S.E., Karlin, R.E., Toolin, L.J., Donahue, D.J., Southon, J.R., Vogel, J.S., 1991. Low organic carbon accumulation rates in Black Sea sediments. Nature 350, 692-695.

Cowie, G.L., Hedges, J.I., 1991. Organic carbon and nitrogen geochemistry of Black Sea sediments spanning the oxic:anoxic boundary, in: Murray, J.W., Izdar, E. (Eds.), Black Sea Oceanography, NATO, Adv. Stud. Inst. Ser., Kluwer, Dordrecht, pp. 343-359.

Crusius, J., Anderson, R.F., 1992a. Inconsistencies in accumulation rates of Black Sea sediments inferred from records of laminae and ^{210}Pb. Paleoceanography 7(2), 215-227.

Crusius, J., Anderson, R.F., 1992b. Immobility of ^{210}Pb in Black Sea sediments. Geochim. Cosmochim. Acta 55, 327-333.

Cutshell, N.H., Larsen, I.L., Olsen, C.R., 1983. Direct analysis of ^{210}Pb in sediment samples: self-absorption correction. Nucl. Inst. Method. 206, 309-317.

Dukat, D.A., Kuehl, S.A., 1995. Non-steady-state ^{210}Pb flux and the use of ^{228}Ra /^{226}Ra as a geochronometer on the Amazon continental shelf. Mar. Geol. 125, 329-350.

Falkner, K. K., O'Neill, D. J., Todd, J. F., Moore, W. S., Edmond, J. M., 1991. Depletion of barium and radium-226 in Black Sea surface waters over the past thirty years. Nature 350, 491-494.

Gulin, S.B., 2000. Recent changes of biogenic carbonate deposition in anoxic sediments of the Black Sea: sedimentary record and climatic implication. Mar. Environ. Res. 49, 319-328.

Gulin, S.B., Polikarpov, G.G., Egorov, V.N., Martin, J.M., Korotkov, A.A., Stokozov, N.A., 2002. Radioactive contamination of the north-western Black Sea sediments. Estuar. Coast. Shelf S. 54, 541-549.

Gulin, S.B., Polikarpov, G.G., Egorov, V.N., 2003. The age of microbial carbonate structures grown at methane seeps in the Black Sea with an implication of dating the seeping methane. Mar. Chem. 84, 67-72.

Fossing, H., Jørgensen, B.B., 1989. Measurement of bacterial sulfate reduction in sediments: evaluation of a single step chromium reduction method. Biogeochemistry 8, 205-222.

Hay, B.J., 1988. Sediment accumulation in the central Eastern Black Sea over the past 5100 years. Paleoceanography 3, 491-508.

Hay, B.J., Honjo, S., 1989. Particle deposition in the present and Holocene Black Sea. Oceanography 2, 26-31.

Jones, G., 1990. AMS radiocarbon dating of sediments and waters from the Black Sea: An integrated approach. EOS Trans. AGU 71, 152.

Jørgensen, B.B., 1979. A theoretical model of stable sulfur isotope distribution in marine sediments. Geochim. Cosmochim. Acta 43, 363–374.

Konovalov, S.K., Luther, G.W., Yücel, M., 2007. Porewater redox processes and sediments in the Black Sea sediments. Chem. Geol. 245, 254-274.

Lyons, T.W., 1997. Sulfur isotopic trends and pathways of iron sulfide formation in upper Holocene sediments of the anoxic Black Sea. Geochim. Cosmochim. Acta 61, 3367–3382.

Lyons, T.W., Kashgarian, M., 2005. Paradigm lost, paradigm found. The Black Sea – black shale connection as viewed from the anoxic basin margin. Oceanography 18 (2), 86-99.

Mitropolsky, A.Y., Bezborodov, A.A., Ovsyany, E.I., 1982. Geochemistry of the Black Sea. Naukova Dumka, Kiev, 144 (In Russian).

Moore, W.S., O'Neill, D., 1991. Radionuclide distributions in recent Black Sea sediments, in: Black Sea Oceanography, NATO ASI Series, Izdar, E., Murray, J.W., (Eds.) Kluwer Academic, Boston, Mass., USA.

Moore, W. S., Falkner, K. K., 1999. Cycling of radium and barium in the Black Sea. J. Environ. Radioactiv. 1999, 247-254.

Neretin, L.N., Böttcher, M.E., Grinenko, V.G., 2003. Sulfur isotope geochemistry of the Black Sea water column. Chem. Geol. 200, 59-69.

Nieuwenhuize, J., Maas, Y.E.M., Middelburg, J.J., 1994. Rapid analysis of organic carbon and nitrogen in particulate materials. Mar. Chem. 45, 217–224.

Oguz, T., Tugrul, S., Kideys, A.E., Ediger, V., Kubilay, N., 2005. Physical and biogeochemical characteristics of the Black Sea. *The Sea*, Vol. 14, Chapter 33, 1331-1369.

Ross, D.A., Degens, E.T. MacIlvaine, J., 1970. Black Sea: Recent sedimentary history. Science 170, 163–165.

Phillips, G.W., Marlow, K.W., 1976. Automatic analysis of gamma-ray spectra from germanium detectors. Nuclear Inst. Methods 137, 525-536.

Teodoru, C.R., Friedl, G., Friedrich, J., Roehl, U., Sturm, M., Wehrli, B., 2007. Spatial distribution and recent changes in carbon, nitrogen and phosporus accumulation in sediments of the Black Sea. Mar. Chem. 105, 52-69.

Wijsman, J.W.M., Middelburg, J.J., Herman, P.M.J., Bottcher, M.E., Heip, C.H.R., 2001. Sulfur and iron speciation in surface sediments along the northwestern margin of the Black Sea. Mar. Chem. 74, 261–278.

Yücel, M., Konovalov, S.K., Moore, T.S., Janzen, C., Luther, G.W., 2010a. Sulfur speciation in the upper Black Sea sediments. Chem. Geol. 269, 364-375.

Yücel, M., Luther, G.W., Moore, W.S., 2010b. Earthquake-induced turbidite deposition as a previously unrecognized sink for hydrogen sulfide in the Black Sea sediments. Mar. Chem. 121, 176-186.

Table 1. Core locations

Station	Latitude, N	Longitude, E	Depth, m	Cruise/Date
B1C1	42° 33'	30° 47'	2159	2001 May-June
B1C2	44° 08'	30° 55'	500	2001 May-June
B1C4	44° 26'	31° 31'	957	2001 May-June
B1C5	42° 30'	30 ° 46'	2159	2001 May-June
B1C6	41° 35'	30° 10'	1780	2001 May-June
8-3	44° 26.97'	33° 31.49'	90	2003 April 27
8-5	43° 08.02'	33° 59.94'	2197	2003 April 28
8-7	42° 47.02'	37° 29.58'	2145	2003 May 01
8-19	41° 29.98'	40° 45.13'	1741	2003 May 03
8-23	42° 02.04'	39° 33.22'	2002	2003 May 04
8-28	42° 28.54'	35° 9.94'	2073	2003 May 05
8-29	42° 10.87'	34° 23.62'	110	2003 May 06
8-30	42° 30.88'	30° 59.8'	2159	2003 May 08
9-2	41° 21.94'	29° 15.01'	87	2003 May
9-8	41° 33'	30° 20'	200	2003 May

Table 2. Mass accumulation rates (MAR), sedimentation velocities (S) and radionuclide inventories for Black Sea sediment cores. 'FL' denotes fluff layer

	inventories, dpm cm^{-2}		MAR g m^{-2} yr^{-1} *, **		S, mm yr^{-1}		FL thickness, cm
Core	**$^{210}Pb_{ex}$**	**^{137}Cs**	**$^{210}Pb_{ex}$**	**^{137}Cs**	**$^{210}Pb_{ex}$**	**^{137}Cs**	
Shelf							
8-3	120	18.3	***	978 ± 140	***	2.1 ± 0.3	
8-29	50.7	13.7	***	390 ± 130	***	0.88 ± 0.3	
9-2	47.3	16.3	***	1673 ± 240	***	2.1 ± 0.3	
Slope							
9-8	18.1	2.21	***	***	***	***	
Basin margin							
B1C6	42.2	5.44	***	***	***	***	
B1C2	7.4	0.01	94 ± 44	***	0.39 ± 0.18	***	
B1C4	9.13	0	106 ± 10	***	0.38 ± 0.04	***	
8-28	74.5	6.91	178 ± 27	257 ± 37	0.47 ± 0.08	2.1 ± 0.3	1
8-19	67.6	23.1	***	2768 ± 111	***	7.4 ± 0.3	2
Abyssal plain							
8-23	84.2	4.78	76 ± 7	117 ± 17	0.48 ± 0.05	2.1 ± 0.3	5
8-7	72.8	2.38	61 ± 6	44 ± 9	0.47 ± 0.05	1.4 ± 0.3	4
8-5	172	2.18	***	93 ± 14	***	2.1 ± 0.3	5
8-30	91.9	12.0	***	5230 ± 125	***	12.4 ± 0.3	1
B1C1	11.6	0.18	72 ± 35	***	0.25 ± 0.13	***	
B1C5	86.0	4.96	***	1120 ± 103	***	3.67 ± 0.3	****

* The error associated with the Pb-based MAR was calculated using the 95% confidence interval of the coefficient "b" in the best-fit equation A(z') = a*exp(bz'), b = -lambda / MAR (see Equation 3 in the text). For the Cs-based MAR, the error was calculated using simply the 0.5 cm depth uncertainty related to each Cs maximum location in the profiles.

** The Pb-based MARs are maximum rates based on the assumptions of the model (section 2.2). The Cs-based MARs, where applicable, give an average rate for the period 1986-2003.

*** MAR/S could not be calculated.
**** Surface lost

Table 3. Mean $\delta^{34}S_{VCDT}$ of the sediments of the deep Black Sea basin. 'n' is the number of depth sections in the core on which isotopic analyses were performed.

Station	n	Mean $\delta^{34}S_{CDT}$, per mil	% St. Dev.
8-19	3	-24.6	12.7
8-23	3	-35.7	5.04
8-7	6	-36.3	17.5
8-30 (1-19cm)	9	-24.0	13.2
8-30 (20-51cm)	9	-31.0	14.8

Figure Captions

Figure 1. Coring locations during the 2001 (B1CX) and 2003 R/V Knorr cruises.

Figure 2. Results of the 2001 cores from the western Black Sea. Note the change in scales.

Figure 3. Results from the 2003 cores. Note the change in scales. Light-gray bands indicate fluff layers defined as sediment layers having porosities >0.96.

Figure 4. Results from 2003 anoxic basin cores. Dashed lines show the turbidites of 8-19 and 8-30 where they are well defined by their radionuclide and geochemical features. Light-gray bands indicate fluff layers defined as sediment layers having porosities >0.96.

Figure 5. Least squares exponential fits (Microsoft Excel) to the core data where Equation 3 was applied for MAR calculation. See Table 2 for the calculated MAR values and associated errors deriving from these best-fit lines.

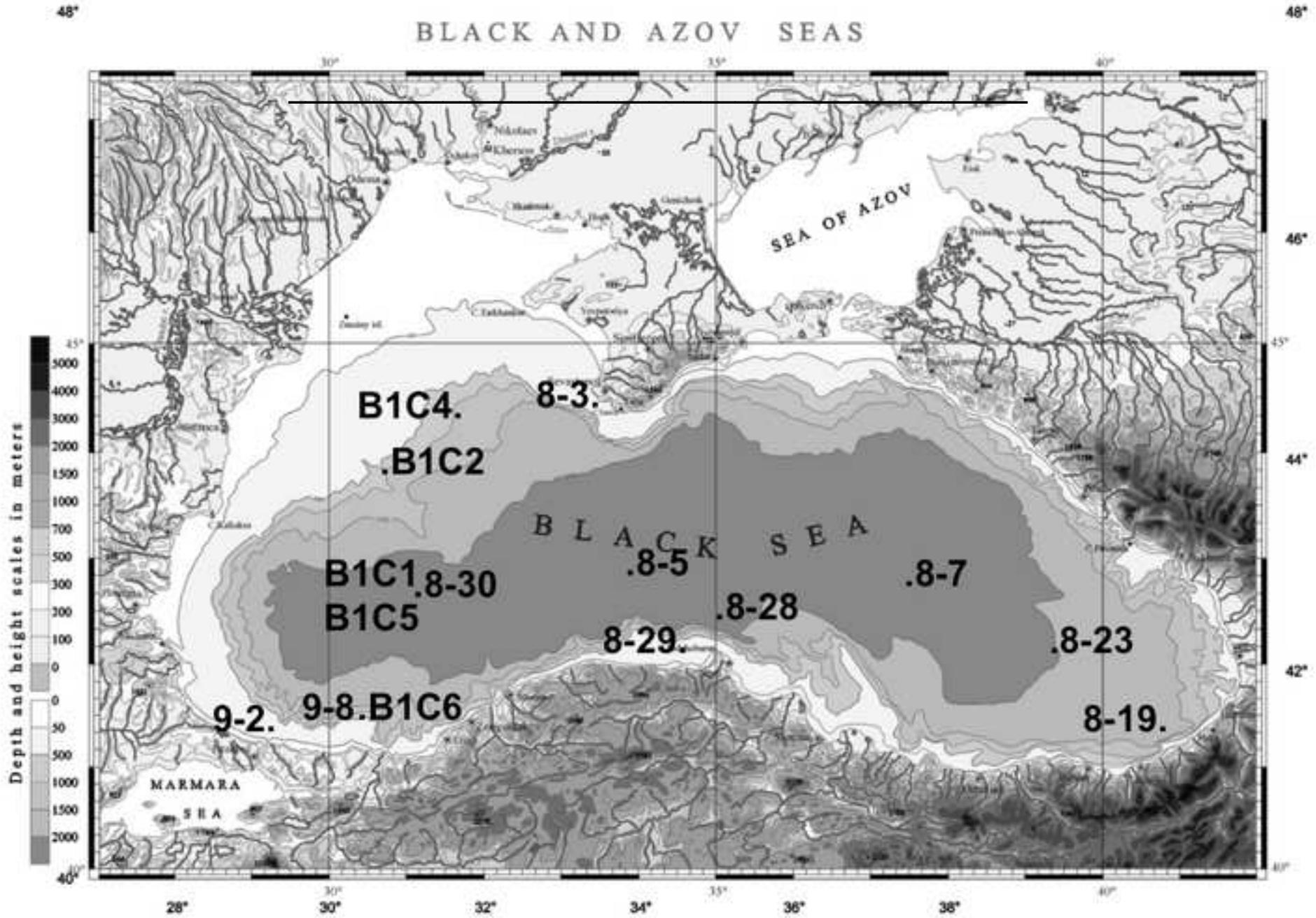
BLACK AND AZOV SEAS
SEA OF AZOV
B L A C K S E A
MARMARA SEA
B1C4.
8-3.
.B1C2
B1C1
.8-30
B1C5
.8-5
.8-7
.8-28
8-29.
.8-23
9-2.
9-8.B1C6
8-19.
Depth and height scales in meters
5000
4000
3000
2000
1500
1000
700
500
300
200
100
0
0
50
500
1000
1500
2000
48°
46°
44°
42°
40°
28°
30°
32°
34°
36°
38°

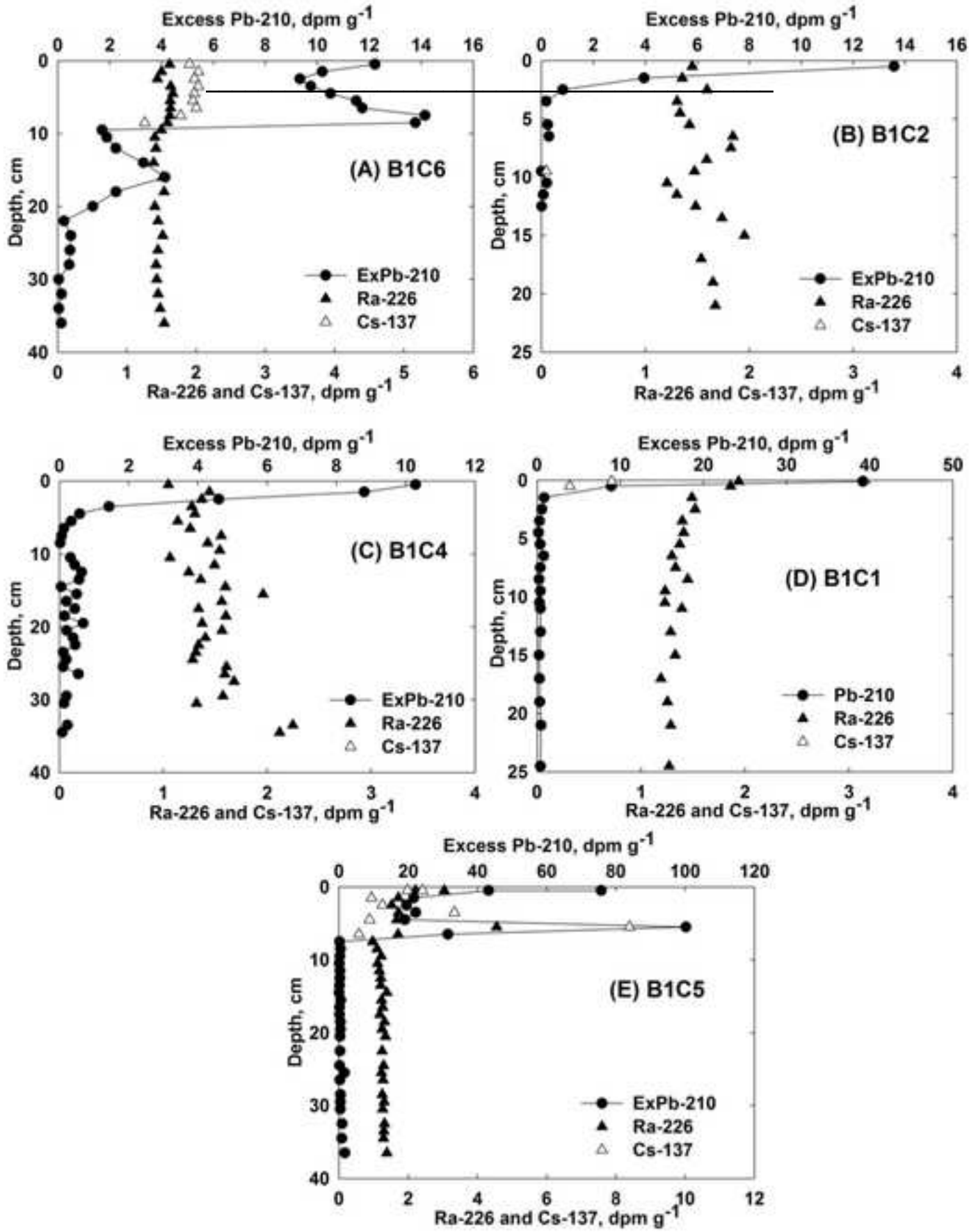
Excess Pb-210, dpm g-1
Depth, cm
(A) B1C6
ExPb-210
Ra-226
Cs-137
Ra-226 and Cs-137, dpm g-1
(B) B1C2
(C) B1C4
(D) B1C1
Pb-210
(E) B1C5

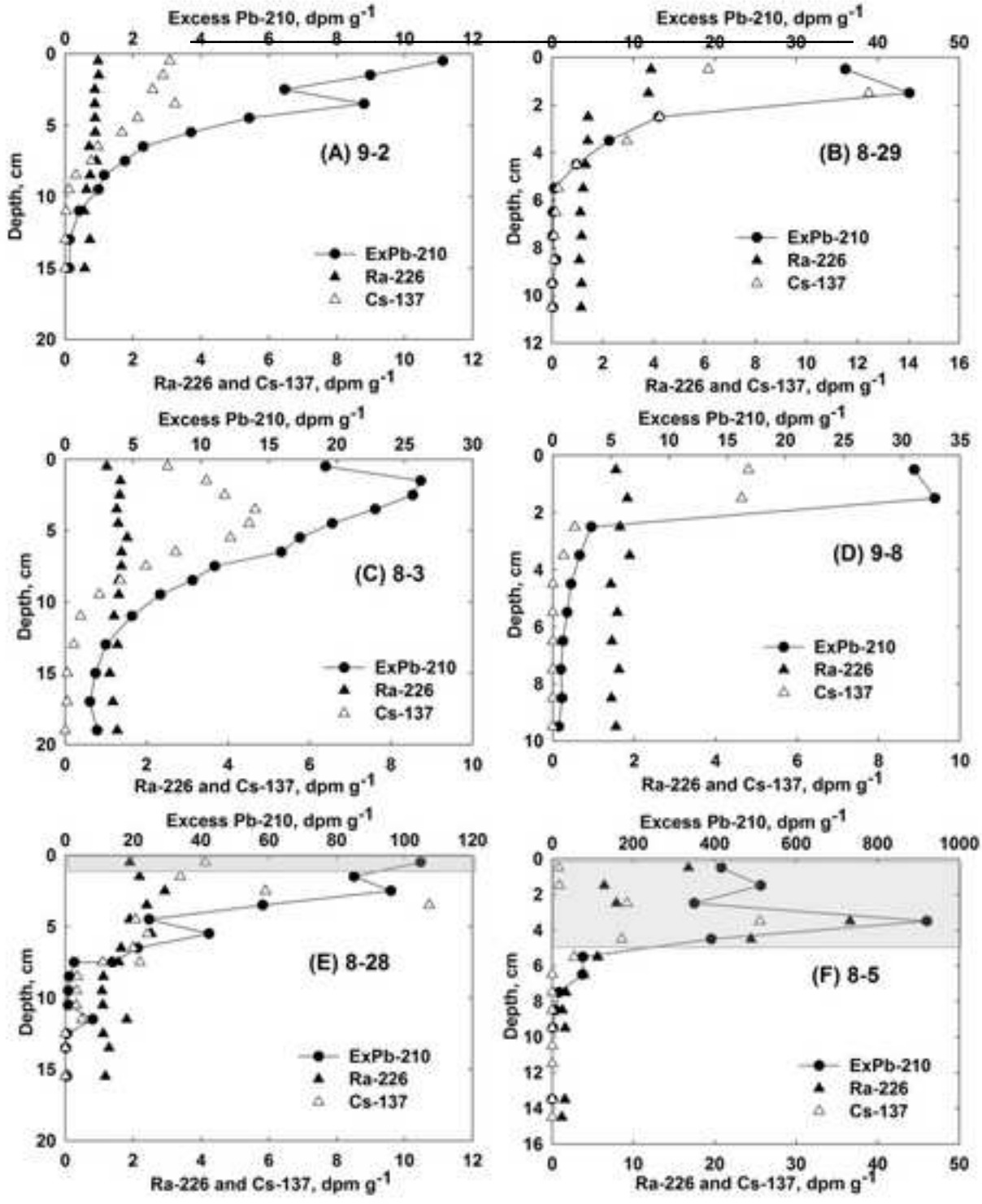
Excess Pb-210, dpm g-1
Depth, cm
Ra-226 and Cs-137, dpm g-1
(A) 9-2
(B) 8-29
(C) 8-3
(D) 9-8
(E) 8-28
(F) 8-5
ExPb-210
Ra-226
Cs-137

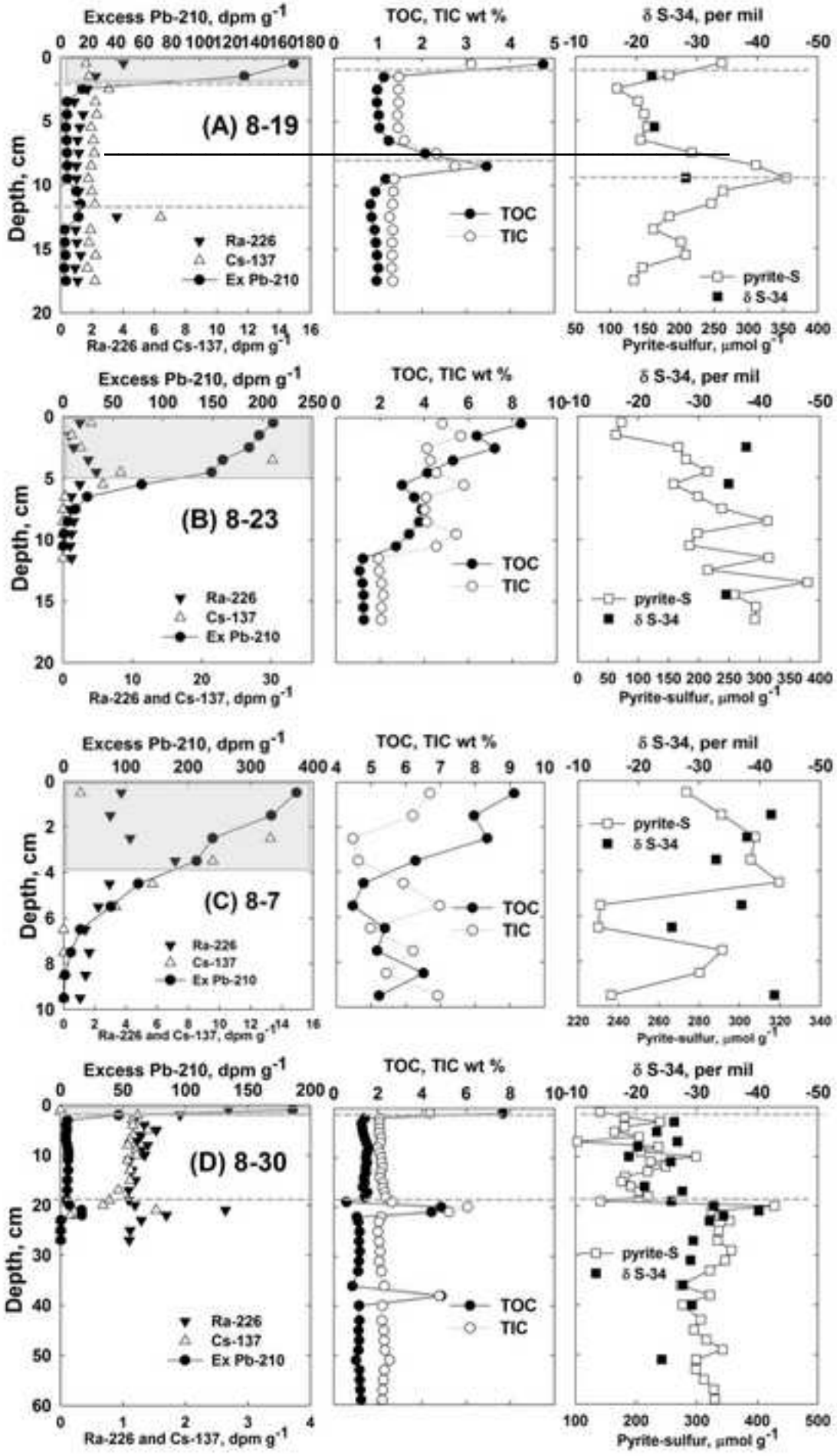
Excess Pb-210, dpm g-1
TOC, TIC wt %
δ S-34, per mil
(A) 8-19
Depth, cm
Ra-226
Cs-137
Ex Pb-210
TOC
TIC
pyrite-S
δ S-34
Ra-226 and Cs-137, dpm g-1
Pyrite-sulfur, μmol g-1
(B) 8-23
(C) 8-7
(D) 8-30

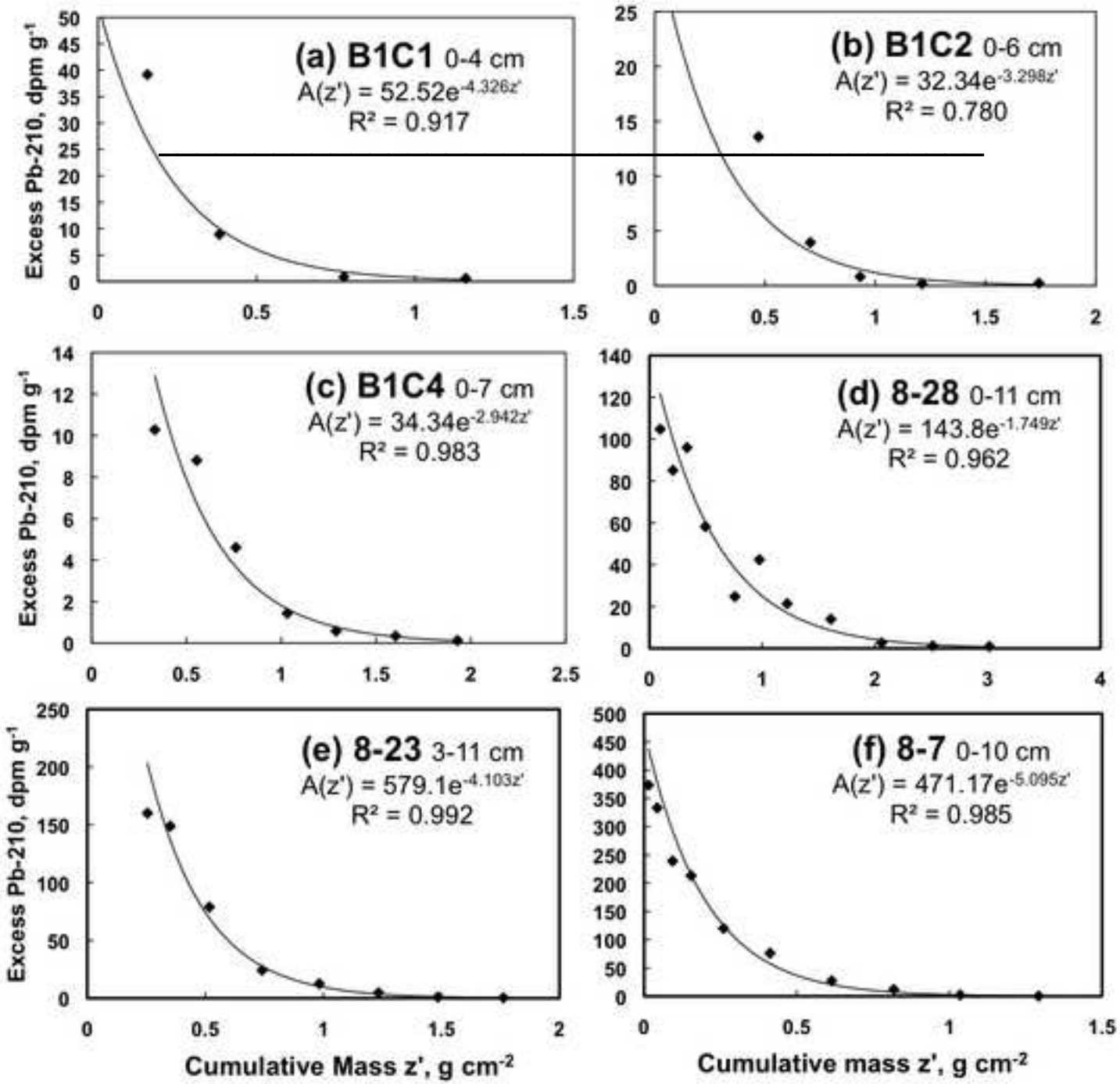
(a) B1C1 0-4 cm
A(z') = 52.52e-4.326z'
R² = 0.917
(b) B1C2 0-6 cm
A(z') = 32.34e-3.298z'
R² = 0.780
(c) B1C4 0-7 cm
A(z') = 34.34e-2.942z'
R² = 0.983
(d) 8-28 0-11 cm
A(z') = 143.8e-1.749z'
R² = 0.962
(e) 8-23 3-11 cm
A(z') = 579.1e-4.103z'
R² = 0.992
(f) 8-7 0-10 cm
A(z') = 471.17e-5.095z'
R² = 0.985
Excess Pb-210, dpm g-1
Cumulative Mass z', g cm-2
Cumulative mass z', g cm-2